Title: Inactivation of endothelial cell phosphoinositide 3-kinase β inhibits tumor angiogenesis and tumor growth

Running title: Endothelial PI3Kβ loss inhibits tumor angiogenesis

Authors: Abul K. Azad[1], Pavel Zhabyeyev[1, 2], Bart Vanhaesebroeck[3], Gary Eitzen[4], Gavin Y. Oudit[1, 2], Ronald B. Moore[5], Allan G. Murray[1]

Affiliations: Departments of [1]Medicine, [2]Physiology, [4]Cell Biology, [5]Oncology, University of Alberta, Edmonton, Canada, and [3]UCL Cancer Institute, University College London, UK.

Corresponding author: Allan G. Murray; email: allan.murray@ualberta.ca; ORCID: https://orcid.org/0000-0003-2131-8192

Keywords: endothelial cell, neovascularization, neoplasm, signal transduction, angiogenesis inhibitor

Abstract

Angiogenesis inhibitors, such as the receptor tyrosine kinase (RTK) inhibitor sunitinib, target vascular endothelial growth factor (VEGF) signaling in cancers. However, only a fraction of patients respond, and most ultimately develop resistance to current angiogenesis inhibitor therapies. Activity of alternative pro-angiogenic growth factors, acting via RTK or G-protein coupled receptors (GPCR), may mediate VEGF inhibitor resistance. The phosphoinositide 3-kinase (PI3K)β isoform is uniquely coupled to both RTK and GPCRs. We investigated the role of endothelial cell (EC) PI3Kβ in tumor angiogenesis. Pro-angiogenic GPCR ligands were expressed by patient-derived renal cell carcinomas (PD-RCC), and selective inactivation of PI3Kβ reduced PD-RCC-stimulated EC spheroid sprouting. EC-specific PI3Kβ knockout (EC-βKO) in mice potentiated the sunitinib-induced reduction in subcutaneous growth of LLC1 and B16F10, and lung metastasis of B16F10 tumors. Compared to single-agent sunitinib treatment, tumors in sunitinib-treated EC-βKO mice showed a marked decrease in microvessel density, and reduced new vessel formation. The fraction of perfused mature tumor microvessels was increased in EC-βKO mice suggesting immature microvessels were most sensitive to combined sunitinib and PI3Kβ inactivation. Taken together, EC PI3Kβ inactivation with sunitinib inhibition reduces microvessel turnover and decreases heterogeneity of the tumor microenvironment, hence PI3Kβ inhibition may be a useful adjuvant anti-angiogenesis therapy with sunitinib.

Introduction

Kidney cancer is among the most common cancers, predominantly affecting those over 45 years, with a lifetime risk of about 2.1% among men and 1.2% among women [1]. A high fraction of these tumors carry a poor prognosis due to metastatic spread at the time of diagnosis [2]. The opportunity for curative surgery is therefore limited, and first-line treatment for these poor-prognosis cancers is directed at inhibition of tumor neo-angiogenesis to indirectly limit tumor growth [2].

Vascular endothelial growth factor (VEGF) is recognized as the dominant growth factor for embryonic vascularization [3]. Similarly, in the adult, malignant cells and tumor stromal cells exploit VEGF to drive vascular endothelial cell (EC) sprouting and expansion from the existing mature vasculature [4-7]. This pathway is targeted by angiogenesis inhibitors, for example neutralizing antibodies to VEGF, or small molecule inhibitors of the VEGF receptor-2 tyrosine kinase (RTK) activity [8]. Treatment with angiogenesis inhibitors results in arrested tumor progression or tumor regression in a fraction of cancer patients [2, 9]. However, this anti-tumor effect is not sustained, and tumor neo-angiogenesis and growth eventually escape drug inhibition [10].

Other pro-angiogenic pathways are thought to be upregulated by the tumor when the VEGF pathway is drug-inhibited [11]. These include Hepatocyte Growth Factor via the c-met RTK among others, which can be targeted by extended-spectrum RTK inhibitors [12]. In contrast, pro-angiogenic ligands for endothelial G-protein coupled receptors

(GPCRs), also expressed by the cancer and tumor stromal cells, are not blocked. These include pro-angiogenic inflammatory chemokines, such as interleukin-8 [13] or chemokine (C-X-C motif) ligand 7 (CXCL7) [14], and developmental angiogenic cues, such as stromal cell derived factor-1/CXCL12 (CXCL12) and apelin [15, 16]. These pro-angiogenic RTK and GPCR pathways converge to efficiently activate mammalian target of rapamycin (mTOR) kinase signaling. Temsirolimus, a salvage anti-angiogenesis agent that inhibits mTOR activity, is approved to treat advanced kidney cancer, but is limited by systemic toxicity [17].

Endothelial phosphoinositide 3-kinase (PI3K) activity couples pro-angiogenic cell surface receptors to mTOR and other effectors such as Akt [18, 19]. PI3K activity in ECs has been shown to be both required and rate-limiting for angiogenesis [20-22]. Among the 3 classes of PI3K, the class I group is the most extensively studied. Aberrant signalling via these enzymes downstream of RTKs, GPCRs, and small GTPases promote many human cancers [23, 24]. The class I PI3Ks comprise four catalytic subunits (p110α, β, γ and δ) that are bound to p85 regulatory subunits [25]. Whereas p110α and p110β show a broad tissue distribution, p110γ and p110δ are mainly found in leukocytes [24]. The p110α isoform is the dominant form coupled to RTKs such as the VEGF receptor-2 (VEGFR2) in EC [20], whereas p110β and p110γ are coupled to pro-angiogenic endothelial GPCRs [20].

In this report we tested the hypothesis that renal cell carcinomas (RCCs) express pro-angiogenic GPCR ligands as alternative cues to VEGF to support tumor neo-angiogenesis. We further examined if selective inhibition of GPCR-stimulated PI3Kβ activity alters neo-angiogenesis and tumor growth under chronic sunitinib-mediated VEGFR2 inhibition.

Material and Methods

Human tissue material

Human renal cell carcinoma tissue samples were obtained at surgical resection of the tumor with the patient's consent under a protocol approved by the Human Research Ethics Board of the University of Alberta. The characteristics of the tumors is summarized in Supplemental Table 1.

Cell culture

HUVEC, B16F10 mouse melanoma, and mouse Lewis lung carcinoma cell lines were cultured as described in Extended Methods (Supplemental Materials).

To investigate the involvement of specific PI3K isoforms, cells were treated for 1 h with the PI3Kα-specific inhibitor BYL-719 (30 nM) or the PI3Kβ-specific inhibitor TGX-221 (100 nM), followed by stimulation of cells with 30 ng/ml VEGF and 50 ng/ml CXCL12 as indicated in the experiment. The data is representative of 3 independent experiments.

Drugs

Sunitinib (Pfizer) was dissolved in 1X PBS (without Ca^{2+} and Mg^{2+}) containing 0.1% DMSO at a concentration 5 mg/ml. This stock solution of sunitinib was kept at 4°C and used within a week. Hypoxyprobe™-1 (NPI Inc) was prepared at a concentration of 100 mg/ml in 0.9% saline and kept at 4°C. TGX-221 (Cayman chemical) was reconstituted in alcohol and further diluted to 100 μM in PBS.

3D angiogenesis assay

In vitro 3D angiogenesis assay was performed as described previously [26, 27]. Each data point reflects one independent PD-RCC/ HUVEC co-culture.

Animal model

Animal experiments were performed following the guidelines approved by the Canadian Council for Animal Care, and the animal protocol was approved by the Animal Care and Use Committee at the Alberta Health Services Cross Cancer Institute.

Mouse Lewis lung carcinoma (LLC1; ATCC) or B16F10 mouse melanoma (ATCC; 1 x 10^6) cells were subcutaneously injected in 12-week-old mixed sex EC-βKO or control mice. Tumor volume was measured every 3 days. Vehicle or sunitinib (40 mg/kg i.p. daily) was started when the tumor volume reached an average size of 200 mm^3. Mice were euthanized at day 16 post injection or when tumor volume reached an average size >1500 mm^3. In the experimental metastasis model, B16F10 mouse melanoma cells (2 x 10^5) were injected into the tail vein of 12 weeks old mice.

Western blot

Tissue lysate from PD-RCC samples or mouse tissues and HUVECs were collected and processed as described in Extended Methods. Each data point reflects one independent PD-RCC/ HUVEC co-culture. A list of the antibodies is in Supplemental Table 2.

RNA isolation and quantitative PCR

Total cell RNA was extracted from HUVECs in 3D-culture or from mouse tumors were processed as described in Extended Methods. Each data point represents an individual mouse. The PCR primers used are listed in Supplemental Table 3.

Immunohistochemistry

Tissue samples were collected in ICH-zinc fixative (BD Bioscience) and kept at room temperature for 48 h, then the samples were paraffin-embedded and 5 μm sections prepared for immunohistochemical analysis. Sections were immunostained for tumor hypoxia (pimonidazole) and tumor vascular density (αCD31; Dianova), pericyte coverage (αNG2; Millipore Sigma; and αPDGFRβ; ThermoFisher Scientific), basement membrane (αCollagen type IV; Millipore Sigma), proliferation marker (αKi67; Abcam), and an apoptosis marker (αCaspase3; Novusbio). Technical details of the processing are described in Extended Methods. Each data point represents an individual mouse.

Statistical analysis

Statistical analyses were performed using GraphPad Prism software. Differences between two groups were analyzed by Mann-Whitney *U* test. Where ANOVA is used, the data were first tested for normality using the D'Agostino test, and found to have similar variance. Primary tumor growth curves of the repeated measure data were analyzed by two-way ANOVA. Error bars represent the mean ± SEM. *P* values < 0.05 were considered significant.

Results

Inhibition of PI3Kβ decreases patient-derived RCC-stimulated sprouting angiogenesis

High-risk renal cell carcinomas are currently managed with anti-angiogenic therapies mainly targeting VEGF-dependent neo-angiogenesis. The role of alternative pro-angiogenic GPCR ligands produced by RCCs or tumor stromal cells to stimulate vascularization of the tumor is poorly defined. We evaluated eight patient-derived RCCs (PD-RCC) obtained by surgical excision, and characterized the ability of these tumors to elicit an angiogenic response from EC spheroids in 3D culture *in vitro* (Fig 1A, B). Four of the eight PD-RCC samples stimulated angiogenic sprouting. Von Hippel-Lindau (VHL) was lost in all tumors that stimulated EC sprouts, but not in the four non-angiogenic PD-RCCs (Supplemental Table 1).

We previously observed that optimal *in vitro* angiogenic sprouting occurs in the context of dual receptor tyrosine kinase and GPCR pro-angiogenic ligands [26]. VEGF-stimulated PI3K-dependent activation of Akt in cultured EC was found to critically depend on PI3Kα, whereas pro-angiogenic CXCL12 signals required PI3Kβ (Supplemental Figure 1; [20]). We next tested the effect of TGX-221, a highly specific inhibitor of PI3Kβ [28], on PD-RCC-stimulated *in vitro* sprouting. Treatment with TGX-221 decreased the number and length of endothelial sprouts in the co-cultures (Figure 1A, B), correlating with reduced expression of *ESM1, DLL4,* and *CXCR4,* genes that mark the lead, or 'tip cell' of an angiogenic sprout [29, 30] (Figure 1C).

Angiogenic PD-RCCs were found to express more VEGF as compared to non-angiogenic PD-RCCs, as analysed by qPCR and western blot (Fig 1D, E). We next probed PD-RCCs for specific pro-angiogenic GPCR ligands such as *CXCL12* and *APLN* (apelin), loss-of-function of which during embryogenesis is associated with defects in vascular development [31, 32]. CXCL12 is predominantly produced by the tumor, whereas apelin is produced by EC. We also examined expression of *CXCL7*, a pro-angiogenic chemokine produced by tumor stromal cells in RCC [14]. Expression of each of these pro-angiogenic growth factors was found to be higher in freshly-isolated angiogenic *versus* non-angiogenic PD-RCC samples, as assessed by qPCR (Figure 1D) or immunoblotting (for VEGF and CXCL12; Figure 1E). TGX-221 treatment did not affect *VEGF*, *CXCL12*, or *APLN* transcript abundance in the co-cultures compared to paired vehicle controls (Supplemental Figure 2). These data show the angiogenic PD-RCCs express both VEGF and pro-angiogenic GPCR ligands, the production of which is independent of PI3Kβ.

EC PI3Kβ KO decreases primary tumor growth

Since endothelial PI3Kβ activity is a convergence node for CXCL12, apelin and CXCL7 GPCR signalling, we sought to determine if EC-selective PI3Kβ loss would alter tumor growth and neo-angiogenesis. Twelve-week old C57Bl/6 *Pik3cb*$^{fl/fl}$/Tie2-CreERT2$^{+/-}$ (EC-βKO) and littermate control C57Bl/6 *Pik3cb*$^{fl/fl}$/Tie2-CreERT2$^{-/-}$ (wild-type) mice

were treated with tamoxifen as described [26], leading to effective Cre-recombinase-mediated disruption of *Pik3cb* (Supplemental Figure 3).

We next implanted Lewis lung carcinoma (LLC1) or B16F10 mouse melanoma cells subcutaneously into the flank of EC-βKO or littermate wild-type mice, followed by treatment with vehicle or the VEGFR2 inhibitor sunitinib when the implanted tumor volume reached an average size of 200 mm^3. This design of the sunitinib treatment has been shown to optimally reduce tumor growth and invasiveness [33]. In agreement with earlier publications, we observed a delay in LLC1 and B16F10 tumor growth in wild-type mice treated with sunitinib (Figure 2A, Supplemental Figure 4). We observed a trend to delayed tumor growth in untreated EC-βKO mice, and further delayed upon sunitinib treatment. These data indicate that inactivation of endothelial PI3Kβ potentiates the reduction in tumor growth obtained with VEGF-pathway inhibition.

EC PI3Kβ KO decreases tumor vascular density

To understand the mechanism of the endothelial PI3Kβ inactivation-mediated delay of primary tumor growth, we examined the tumor microvasculature in sunitinib-treated EC-βKO and wild-type mice. In agreement with previous reports, we found that the density of $CD31^+$ tumor microvessels was decreased in sunitinib-treated wild-type mice (Figure 2B, C, Supplemental Figure 5). Endothelial PI3Kβ inactivation combined with sunitinib treatment further reduced tumor vascularization *versus* sunitinib treatment or endothelial

PI3Kβ inactivation alone. This was associated with increased tumor cell apoptosis, quantified by active caspase 3 immunostaining (Supplemental Figure 6).

Next, we evaluated the impact of EC-PI3Kβ KO on tumor hypoxia in late tumors at the time of maximum tumor growth (1500 mm^3). As anticipated, the reduced tumor vascularization in sunitinib-treated mice was associated with reduced nutrient delivery and increased tumor hypoxia compared to vehicle-treated wild-type mice (Figure 2D, E). We observed a reduction in the pimonidazole-positive hypoxic tumor area in sunitinib-treated EC-βKO *versus* wild-type mice (Figure 2D, E). We further evaluated the expression of the hypoxia-dependent marker genes, glucose transporter 1 (*Glut1*) and N-myc downstream-regulated gene (*Ndrg1*), in the late stage tumors. The abundance of both *Glut1* and *Ndrg1* transcripts was increased in tumors from sunitinib-treated mice (Figure 2F), consistent with the data from the pimonidazole staining. Expression of *Glut1* and *Ndrg1* was reduced in sunitinib-treated-EC-βKO mice *versus* -wild-type mice.

We investigated day 16 (early) post-implantation sunitinib-treated tumors, a timepoint that corresponds to maximal tumor growth in untreated littermate wild-type mice, to better define the effect of endothelial PI3Kβ loss during tumor growth. In wild-type mice, tumor expression of the hypoxia reporter genes was higher in sunitinib-treated than untreated tumors at the similar timepoint, despite the smaller volume of the sunitinib-treated tumors. Endothelial PI3Kβ inactivation mitigated this effect of sunitinib treatment. We found decreased *Ndrg1* and a trend for decreased *Glut1* expression in EC-

βKO *versus* wild-type mice (Figure 2F). We confirmed this finding by western blot of early tumors recovered from sunitinib-treated mice (Figure 2G, H). Moreover, since hypoxia drives expression of *Vegfa*, *Cxcl12* and *Apln*, we examined transcript abundance of these proangiogenic genes. We found that expression of *Vegfa*, *Cxcl12*, and *Apln* were each reduced in tumors in sunitinib-treated EC-βKO mice *versus* -wild-type mice at the early and late stage of tumor growth (Supplemental Figure 7). Together, these data show that while combined endothelial PI3Kβ inactivation and sunitinib treatment maximally slowed tumor growth and decreased microvascular density, endothelial PI3Kβ inactivation reduced tumor hypoxia *versus* sunitinib treatment alone at early and late timepoints in tumor growth.

EC PI3Kβ KO decreases tumor vessel remodeling

The observation that EC PI3Kβ inactivation decreased tumor microvascular density and tumor hypoxia, indicated that endothelial PI3Kβ inactivation may favor tumor vessel normalization, which is characterized by pericyte coverage that stabilizes blood vessels [7]. To gain insight into this, we evaluated pericyte association with $CD31^+$ microvessels using the pericyte markers, NG2 and PDGFRβ, to identify mature, stabilized vessels in late-growth tumors. Our analyses showed that the fraction of both NG2-positive (Figure 3A, B, Supplemental Figure 5B) and PDGFRβ-positive (Supplemental Figure 8A, B, 5C) tumor microvessels was higher in EC-βKO mice compared to wild-type controls. Furthermore, larger tumor 'mother' vessels were also well-covered by pericytes in EC-βKO mice compared to wild-type mice (Supplemental Figure 8C, D, Supplemental

Figure 5C). Consistent with these findings, we observed that tumor *Pdgfb* expression, a major pericyte growth factor and chemoattractant [34], was elevated in tumors from EC-βKO mice (Supplemental Figure 8E).

We further assessed if endothelial PI3Kβ inactivation altered tumor microvessel remodelling. First, we quantified the fraction of $CD31^+$ EC microvessels associated with collagen IV staining, marking maturing microvessels. We found sunitinib treatment reduced the fraction of mature EC $CD31^+$ microvessels covered by collagen IV^+ basement membranes in wild-type mice (Figure 3C, D left panel). However, loss of endothelial PI3Kβ was associated with a normalization of the fraction of mature tumor microvessels in sunitinib-treated mice (Figure 3C, D left panel).

Regression of established microvessels is associated with remnant basement membrane sleeves from which ECs have been lost [35]. Sunitinib treatment markedly increased the fraction of collagen IV^+ remnant vessel profiles lacking an endothelium in wild-type mice (Figure 3C, D right panel). However, we observed a reduction in the number of remnant microvessel basement membrane sleeves in the tumors of sunitinib-treated EC-βKO mice (Figure 3C, D right panel). Moreover, remnant vessel profiles were also reduced in the tumors from carrier-treated EC-βKO mice. Together, these data indicate that VEGFR2 inhibition is associated with a high turnover of immature tumor microvessels. Endothelial PI3Kβ loss blunts both immature vessel initiation or stability, and regression of mature microvessels.

We next assessed the effect of endothelial PI3Kβ inactivation on vessel perfusion under sunitinib treatment. We studied early post-implant tumors from sunitinib-treated mice. Consistent with our evaluation of the late-growth tumors, endothelial loss of PI3Kβ was associated with a reduction in microvessel density (Figure 3E, F upper panel, Supplemental Figure 5B). However, the fraction of perfused microvessels, labelled by antemortem intravenous lectin staining, was increased in the EC-βKO *versus* wild-type control mice (Figure 3E, F lower panel). These data indicate that inactivation of endothelial PI3Kβ further reduces sunitinib-induced microvascular remodelling, promotes tumor vessel normalization, and increases the net fraction of perfused vessels.

EC PI3Kβ KO suppresses sprout formation

We observed that TGX-221-mediated inhibition of PI3Kβ reduced *in vitro* endothelial spheroid sprouting in PD-RCC co-cultures (Fig 1). We therefore examined the effect of endothelial PI3Kβ inactivation on tumor microvessel sprouting *in vivo*. As shown in Figure 4, A, B and Supplemental Figure 5D, sunitinib treatment was associated with a reduction in sprouts from tumor mother vessels. Combined endothelial PI3Kβ inactivation and sunitinib treatment was associated with a further reduction in sprout formation (Figure 4A, B and Supplemental Figure 5D). We characterized angiogenic endothelial tip cell marker-gene expression among the tumors from sunitinib-treated mice in both early- and late-growth post-implant tumors. We found EC PI3Kβ inactivation co-

ordinately reduced the expression of *ESM1*, *DLL4* and *CXCR4 versus* wild-type hosts, in tumors from sunitinib-treated mice (Figure 4C). Tip cell gene expression in the tumors was reduced in the EC-βKO *versus* the wild-type mice at both the early and late growth sunitinib-treated mice. This suggests that delayed tumor growth and reduced microvessel density in sunitinib-treated EC-βKO mice is associated with a sustained decrease in tumor sprouting neo-angiogenesis. Further, we evaluated tumor angiopoietin-2 expression, another characteristic tip cell marker, by western blot in early tumors from sunitinib-treated mice. We observed that angiopoietin-2 was reduced in tumors from ECβ-KO *versus* wild-type sunitinib-treated mice. Similarly, ESM1 matrix protein deposits were reduced in tumors from the EC-βKO *versus* wild-type tumors (Supplemental Figure 9, 5E). These data indicate that inactivation of endothelial PI3Kβ activity in combination with sunitinib-mediated VEGFR2 inhibition, markedly reduces neo-vessel sprouting and microvessel density, while sparing pericyte-covered established vessels.

EC PI3Kβ KO dampens sunitinib-associated tumor cell epithelial to mesenchymal transition

Our data show that endothelial PI3Kβ loss combined with sunitinib treatment optimally reduces microvessel density, tumor growth, and promotes tumor apoptosis. Next, we evaluated the effect of sunitinib treatment with and without endothelial PI3Kβ deficiency on the tumor cells. We observed a decreased frequency of Ki-67^{+} proliferating cells in tumor cortex from ECβ-KO *versus* wild-type sunitinib-treated mice (Supplemental

Figure 10, 5F). We further evaluated if vascular normalization in EC-βKO mice reduced tumor cell epithelial-to-mesenchymal transition (EMT), a process that is involved in tumor progression and metastatic spread to distant sites [36]. To test this, we determined the expression of the EMT-driving transcription factors, *Twist1*, *Zeb1*, *Snail1* and *Slug* [36]. Sunitinib treatment markedly upregulated expression of these transcription factors in late growth tumors in wild-type mice (Figure 5A). Expression of each of these transcription factors was lower in tumors from EC-βKO *versus* wild-type control sunitinib-treated mice, in both early and late growth tumors (Figure 5A). Further, we evaluated Zeb1 and Slug expression by western blot in early growth tumors. We confirmed reduced expression in tumors from EC-βKO *versus* wild-type sunitinib-treated mice. Together, these data indicate that EC PI3Kβ inactivation with sunitinib treatment optimally reduces tumor cell proliferation, and blunts sunitinib treatment-associated EMT.

EC PI3Kβ KO reduces tumor metastasis

Tumor growth at metastatic sites requires tumor cell seeding in the naïve vascular bed, with subsequent growth dependent on neo-angiogenesis or co-option of the native microvasculature [37]. VEGF inhibitor treatment has been implicated to sensitize the lung vasculature to support tumor cell extravasation [38]. We evaluated the effect of endothelial PI3Kβ inactivation in the metastatic seeding potential of B16F10 mouse melanoma cells under sunitinib treatment. B16F10 cells were injected into the tail vein of 12-15 week EC-βKO or littermate wild-type mice. Sunitinib alone did not affect tumor

metastasis (Figure 6A). However, endothelial PI3Kβ inactivation resulted in reduced tumor foci establishment in the lung, and decreased tumor area per lung in EC-βKO mice *versus* wild-type mice (Figure 6A, B; Supplemental Figure 11 A, B). Similar to the LLC1 primary tumor model, B16F10 metastases showed a decrease in $CD31^+$ microvessels in sunitinib-treated EC-βKO *versus* -wild-type mice (Figure 6C, D, Supplemental Figure 5G). This was accompanied by a reduction in endothelial tip cell marker gene expression, consistent with a reduction in sprouting neo-angiogenesis (Supplemental Figure 12). Furthermore, the pimonidazole-positive hypoxic area in the metastatic tumors was substantially reduced in sunitinib-treated tumors from ECβ-KO *versus* wild-type mice (Figure 6E, F). Consistent with the subcutaneous primary LLC tumor model, a greater fraction of microvessels were found to be covered with pericytes in sunitinib-treated tumors from the ECβ-KO *versus* wild-type mice (Figure 6G, H). These data indicate that metastatic B16F10 tumor growth and angiogenesis is optimally reduced by combined endothelial PI3Kβ inactivation with sunitinib-mediated VEGF receptor inhibition.

Discussion

The anticipated benefit of angiogenesis inhibition therapies to control advanced or chemotherapy-resistant cancer is not fully realized, since not all tumors respond to anti-VEGF treatment, and those that do initially respond eventually become resistant [39]. Further, the unstable immature vessels associated with anti-VEGF treatment may compromise the delivery and effect of chemotherapy or immune-modulating anti-tumor drugs. This is particularly important, since emerging clinical trial data suggests that a

combination of angiogenesis inhibitors and immune-modulating agents optimizes outcomes *versus* either approach alone [40, 41].

In this study, we sought to understand the role of pro-angiogenic ligands for endothelial GPCRs in tumor neo-angiogenesis. We show that a subset of patient-derived RCC samples are able to elicit angiogenic sprouting from endothelial spheroids *in vitro*. These PD-RCCs express VEGF as well as pro-angiogenic ligands (*CXCL12*, *CXCL7*, and *APLN*) for endothelial GPCRs. Inhibition of PI3Kβ, a common signal integration node for GPCRs, in these co-cultures did not reduce pro-angiogenic growth factor gene expression by the cancer and stromal cells, but inhibited tumor-driven angiogenic sprouting. These data suggest these mediators participate to cue tumor EC neo-angiogenesis in humans, acting through endothelial PI3Kβ.

We directly tested this idea in mice by inactivating PI3Kβ selectively in the host endothelium, then evaluated tumor growth under anti-VEGF receptor-2-treatment. PI3Kβ inactivation alone reduced subcutaneous growth of LLC1 and B16F10 tumors. Further, endothelial PI3Kβ KO markedly potentiated sunitinib-driven growth inhibition of both LLC1 and B16F10 tumors in mice. This finding is supported by an increase in cleaved caspase-3^+ apoptotic tumor cells, and reduced fraction of Ki-67^+ proliferating tumor cells, in tumors with combined endothelial PI3Kβ inactivation and VEGF receptor-2 inhibition. Sunitinib treatment alone reduced tumor microvessel density and markedly increased tumor hypoxia, expression of hypoxia reporter genes, and tumor EMT in late-growth

tumors. EC PI3Kβ inactivation combined with sunitinib treatment mitigated tumor hypoxia, hypoxia-responsive gene expression, and expression of the EMT markers *versus* sunitinib treatment alone in early and late stage tumors. Earlier work has shown the effects of VEGF receptor-2 inhibition to reduce tumor neoangiogenesis and vascular density and yet increase tumor oxygenation are transient [42, 43]. Stabilization of the tumor microvasculature, mediated by combined endothelial PI3Kβ and VEGFR2 inactivation, reduces vascular heterogeneity in the early and late tumor microenvironment consistent with a sustained decrease in cyclic tumor hypoxia. Hypoxic niches in the tumor have been linked to a cancer cell EMT program that may facilitate metastasis or resistance to chemotherapy[44, 45]. Our data suggest cyclic tumor hypoxia associated with immature microvessel turnover is an important driver of LLC cancer cell EMT that can be mitigated by dual inactivation of proangiogenic RTK and GPCR signalling.

Tumor microvessels in the late-growth tumors from ECβ-KO hosts were found to be more mature, covered by both basement membranes and pericytes, with tumors featuring fewer empty basement membrane sleeves arising from regressed microvessels [35]. The combination of endothelial PI3Kβ inactivation and sunitinib-mediated VEGF receptor-2 inhibition suppressed sprouting from tumor mother vessels better than VEGF receptor-2 inhibition alone, consistent with the effect of pharmacological PI3Kβ inhibition in the *in vitro* model of patient-derived RCC angiogenesis. Expression of endothelial tip cell genes was consistently lower in early and late growth tumors from ECβ-KO hosts. The finding was confirmed by the observation that angiopoietin-2 was decreased in the early growth

sunitinib-treated tumors in ECβ-KO hosts. These data suggest that both VEGF and non-VEGF angiogenic cues drive angiogenesis in these tumors. Moreover, these four lines of evidence support the interpretation that compared to mature microvessels, tip cell differentiation and sprout formation are particularly sensitive to the combination blockade of VEGF receptor-2 and pro-angiogenic GPCR cues dependent on PI3Kβ. The net result is a higher fraction of the tumor vessels are perfused if endothelial PI3Kβ is inactivated.

Under VEGF pathway inhibition, cancer or tumor stromal cell [46, 47] recruitment of neovascularization using alternative pro-angiogenic RTK ligands contributes to acquired drug resistance [48, 49], and is partially mitigated by the broader receptor inhibition profile of new-generation anti-angiogenic agents such as cabozantinib [12]. However, RTK antagonists do not inhibit pro-angiogenic GPCR ligands generated by cancer or stromal cells. Earlier work has identified upregulation of ligands such as CXCL12, IL-8, and CXCL-7 that might contribute to neovascularization under VEGF/VEGF receptor blockade [14, 50, 51]. Moreover, autocrine apelin receptor signaling in angiogenic ECs participates in developmental and tumor angiogenesis [52, 53]. Since tumors are heterogeneous for these and other mediators, our data suggest that targeting an important common GPCR signal integration node in the EC, such as PI3Kβ, may complement RTK inhibitors of angiogenesis.

Neo-angiogenesis and dysfunctional vascular remodelling are associated with progression and metastasis of several cancer types [54]. The effects of anti-angiogenesis drugs, such as sunitinib, on the tumor microvasculature promote non-homogeneous oxygen and nutrient delivery that results in microenvironmental niches favoring cancer cell transition to more aggressive forms [38, 55]. In addition, these experimental findings suggest anti-VEGF pathway inhibitors may condition the systemic vasculature to facilitate metastatic cancer cell spread [38]. Combined inhibition of VEGF RTK and PI3Kβ normalized tumor hypoxia-responsive, and EMT gene expression *versus* sunitinib alone. In addition, we observed reduced expression of *Vegf* and *Cxcl12* in these tumors, suggesting re-inforced angiogenesis inhibition upon combined sunitinib and PI3Kβ inactivation. Future experiments will be needed to determine if such combination treatment reduces metastatic behaviour of the primary tumor. However, we find that this regimen reduced tumor seeding, growth and hypoxia, and promoted tumor microvessel maturation in the B16 lung metastasis model. These data suggest combined inhibition favourably promotes host microvessel resistance to metastasis.

In the endothelium, PI3Kα is coupled to the VEGF RTK, and is indirectly inhibited by VEGF pathway inhibitors. In contrast to endothelial PI3Kβ inhibition, however, PI3Kα inactivation is associated with chaotic tumor neoangiogenesis [56], in part mediated by impaired expression of DLL4 NOTCH ligand, in turn associated with uncontrolled endothelial tip cell differentiation [29]. A reduction in gene expression markers for endothelial tip cells, combined with a reduction in remnant, non-vascularized microvessels in tumors in the sunitinib-treated EC-βKO mice suggests that pro-

angiogenic GPCR ligands functionally drive tumor neoangiogenesis in these models, and contribute to unbalanced PI3K isoform signaling.

In summary, our findings in pre-clinical models reveal the potential benefit of combined inhibition of VEGF RTK and PI3Kβ to inhibit tumor growth. Freshly-isolated human RCCs were found to express several pro-angiogenic GPCR ligands that can couple to endothelial PI3Kβ, and PD-RCC-stimulated angiogenesis was sensitive to pharmacological PI3Kβ inhibition. This suggests that PI3Kβ inhibition to target the subset of such human tumors merits further investigation. Systemic PI3Kβ inhibition in human cancer has been found to be well-tolerated [57]. Our data suggest that clinical PI3Kβ inhibitors could be useful as an adjuvant to VEGF-based anti-tumor therapies.

Acknowledgements: AA was supported by a Translational Research Fellowship award from the Department of Medicine at the University of Alberta. Operating funding was provided by the Canadian Cancer Society Research Institute to AGM. The authors acknowledge the technical assistance of Jessica DesAulniers.

Potential conflict of interest: B.V. is a consultant for Karus Therapeutics (Oxford, UK), iOnctura (Geneva, Switzerland) and Venthera (Palo Alto, US) and has received speaker fees from Gilead (Foster City, US). The other authors declare no conflict of interest relating to this work.

Author contributions: Concept AKA, GE, GYO, RBM, AGM; Methodology AKA, PZ; Data acquisition AKA; Analysis AKA, AGM; Reagents BV, RBM; Writing AKA, BV, AGM.

References

1 Siegel RL, Miller KD, Jemal A. Cancer statistics, 2019. *CA Cancer J Clin* 2019; 69: 7-34.

2 Choueiri TK, Motzer RJ. Systemic Therapy for Metastatic Renal-Cell Carcinoma. *N Eng J Med* 2017; 376: 354-366.

3 Ferrara N, Carver-Moore K, Chen H, Dowd M, Lu L, O'Shea KS *et al*. Heterozygous embryonic lethality induced by targeted inactivation of the VEGF gene. *Nature* 1996; 380: 439-442.

4 Yuan F, Chen Y, Dellian M, Safabakhsh N, Ferrara N, Jain RK. Time-dependent vascular regression and permeability changes in established human tumor xenografts induced by an anti-vascular endothelial growth factor/vascular permeability factor antibody. *Proc Natl Acad Sci U S A* 1996; 93: 14765-14770.

5 Grunstein J, Roberts WG, Mathieu-Costello O, Hanahan D, Johnson RS. Tumor-derived expression of vascular endothelial growth factor is a critical factor in tumor expansion and vascular function. *Cancer Res* 1999; 59: 1592-1598.

6 Stockmann C, Doedens A, Weidemann A, Zhang N, Takeda N, Greenberg JI *et al*. Deletion of vascular endothelial growth factor in myeloid cells accelerates tumorigenesis. *Nature* 2008; 456: 814-818.

7 De Palma M, Biziato D, Petrova TV. Microenvironmental regulation of tumour angiogenesis. *Nat Rev Cancer* 2017; 17: 457-474.

8 Gougis P, Wassermann J, Spano JP, Keynan N, Funck-Brentano C, Salem JE. Clinical pharmacology of anti-angiogenic drugs in oncology. *Crit Rev Oncol Hematol* 2017; 119: 75-93.

9 Thomas JS, Kabbinavar F. Metastatic clear cell renal cell carcinoma: A review of current therapies and novel immunotherapies. *Crit Rev Oncol Hematol* 2015; 96: 527-533.

10 Casanovas O, Hicklin DJ, Bergers G, Hanahan D. Drug resistance by evasion of antiangiogenic targeting of VEGF signaling in late-stage pancreatic islet tumors. *Cancer Cell* 2005; 8: 299-309.

11 Jimenez-Valerio G, Casanovas O. Antiangiogenic resistance: novel angiogenesis axes uncovered by antiangiogenic therapies research. *Curr Drug Targets* 2016; 17: 1728-1734.

12 Zhou L, Liu XD, Sun M, Zhang X, German P, Bai S *et al*. Targeting MET and AXL overcomes resistance to sunitinib therapy in renal cell carcinoma. *Oncogene* 2016; 35: 2687-2697.

13 Grepin R, Guyot M, Jacquin M, Durivault J, Chamorey E, Sudaka A *et al*. Acceleration of clear cell renal cell carcinoma growth in mice following bevacizumab/Avastin treatment: the role of CXCL cytokines. *Oncogene* 2012; 31: 1683-1694.

14 Grepin R, Guyot M, Giuliano S, Boncompagni M, Ambrosetti D, Chamorey E *et al*. The CXCL7/CXCR1/2 axis is a key driver in the growth of clear cell renal cell carcinoma. *Cancer Res* 2014; 74: 873-883.

15 Orimo A, Gupta PB, Sgroi DC, Arenzana-Seisdedos F, Delaunay T, Naeem R *et al*. Stromal fibroblasts present in invasive human breast carcinomas promote tumor growth and angiogenesis through elevated SDF-1/CXCL12 secretion. *Cell* 2005; 121: 335-348.

16 Seaman S, Stevens J, Yang MY, Logsdon D, Graff-Cherry C, St Croix B. Genes that distinguish physiological and pathological angiogenesis. *Cancer Cell* 2007; 11: 539-554.

17 Hudes G, Carducci M, Tomczak P, Dutcher J, Figlin R, Kapoor A *et al*. Temsirolimus, interferon alfa, or both for advanced renal-cell carcinoma. *N Engl J Med* 2007; 356: 2271-2281.

18 Ackah E, Yu J, Zoellner S, Iwakiri Y, Skurk C, Shibata R *et al*. Akt1/protein kinase Balpha is critical for ischemic and VEGF-mediated angiogenesis. *J Clin Invest* 2005; 115: 2119-2127.

19 Phung TL, Ziv K, Dabydeen D, Eyiah-Mensah G, Riveros M, Perruzzi C *et al*. Pathological angiogenesis is induced by sustained Akt signaling and inhibited by rapamycin. *Cancer Cell* 2006; 10: 159-170.

20 Graupera M, Guillermet-Guibert J, Foukas LC, Phng LK, Cain RJ, Salpekar A *et al*. Angiogenesis selectively requires the p110alpha isoform of PI3K to control endothelial cell migration. *Nature* 2008; 453: 662-666.

21 Huang J, Kontos CD. PTEN modulates vascular endothelial growth factor-mediated signaling and angiogenic effects. *J Biol Chem* 2002; 277: 10760-10766.

22 Hamada K, Sasaki T, Koni PA, Natsui M, Kishimoto H, Sasaki J *et al*. The PTEN/PI3K pathway governs normal vascular development and tumor angiogenesis. *Genes Dev* 2005; 19: 2054-2065.

23 Zhao L, Vogt PK. Class I PI3K in oncogenic cellular transformation. *Oncogene* 2008; 27: 5486-5496.

24 Bilanges B, Posor Y, Vanhaesebroeck B. PI3K isoforms in cell signalling and vesicle trafficking. *Nat Rev Mol Cell Biol* 2019; 20: 515-534.

25 Vanhaesebroeck B, Whitehead MA, Pineiro R. Molecules in medicine mini-review: isoforms of PI3K in biology and disease. *J Mol Med (Berl)* 2016; 94: 5-11.

26 Haddad G, Zhabyeyev P, Farhan M, Zhu LF, Rayner DC, Vanhaesebroeck B *et al*. PI3K-beta mediates microvascular endothelial repair of thrombotic microagiopathy. *Blood* 2014; 124: 2142-2149.

27 Nowak-Sliwinska P, Alitalo K, Allen E, Anisimov A, Aplin AC, Auerbach R *et al*. Consensus guidelines for the use and interpretation of angiogenesis assays. *Angiogenesis* 2018; 21.

28 Jackson SP, Schoenwaelder SM, Goncalves I, Nesbitt WS, Yap CL, Wright CE *et al*. PI 3-kinase p110beta: a new target for antithrombotic therapy. *Nat Med* 2005; 11: 507-514.

29 del Toro R, Prahst C, Mathivet T, Siegfried G, Kaminker JS, Larrivee B *et al*. Identification and functional analysis of endothelial tip cell-enriched genes. *Blood* 2010; 116: 4025-4033.

30 Strasser GA, Kaminker JS, Tessier-Lavigne M. Microarray analysis of retinal endothelial tip cells identifies CXCR4 as a mediator of tip cell morphology and branching. *Blood* 2010; 115: 5102-5110.

31 Tachibana K, Hirota S, Iizasa H, Yoshida H, Kawabata K, Kataoka Y *et al*. The chemokine receptor CXCR4 is essential for vascularization of the gastrointestinal tract. *Nature* 1998; 393: 591-594.

32 Kasai A, Shintani N, Kato H, Matsuda S, Gomi F, Haba R *et al*. Retardation of retinal vascular development in apelin-deficient mice. *Arterioscler Thromb Vasc Biol* 2008; 28: 1717-1722.

33 Ebos JM, Lee CR, Christensen JG, Mutsaers AJ, Kerbel RS. Multiple circulating proangiogenic factors induced by sunitinib malate are tumor-independent and correlate with antitumor efficacy. *Proc Natl Acad Sci U S A* 2007; 104: 17069-17074.

34 Abramsson A, Lindblom P, Betsholtz C. Endothelial and nonendothelial sources of PDGF-B regulate pericyte recruitment and influence vascular pattern formation in tumors. *J Clin Invest* 2003; 112: 1142-1151.

35 Mancuso MR, Davis R, Norberg SM, O'Brien S, Sennino B, Nakahara T *et al*. Rapid vascular regrowth in tumors after reversal of VEGF inhibition. *J Clin Invest* 2006; 116: 2610-2621.

36 Brabletz T, Kalluri R, Nieto MA, Weinberg RA. EMT in cancer. *Nat Rev Cancer* 2018; 18: 128-134.

37 Bridgeman VL, Vermeulen PB, Foo S, Bilecz A, Daley F, Kostaras E *et al*. Vessel co-option is common in human lung metastases and mediates resistance to anti-angiogenic therapy in preclinical lung metastasis models. *J Pathol* 2017; 241: 362-374.

38 Ebos JM, Lee CR, Cruz-Munoz W, Bjarnason GA, Christensen JG, Kerbel RS. Accelerated metastasis after short-term treatment with a potent inhibitor of tumor angiogenesis. *Cancer Cell* 2009; 15: 232-239.

39 Sennino B, McDonald DM. Controlling escape from angiogenesis inhibitors. *Nat Rev Cancer* 2012; 12: 699-709.

40 McDermott DF, Huseni MA, Atkins MB, Motzer RJ, Rini BI, Escudier B *et al*. Clinical activity and molecular correlates of response to atezolizumab alone or in combination with bevacizumab versus sunitinib in renal cell carcinoma. *Nat Med* 2018; 24: 749-757.

41 Bergerot P, Lamb P, Wang E, Pal SK. Cabozantinib in combination with immunotherapy for advanced renal cell carcinoma and urothelial carcinoma: rationale and clinical evidence. *Mol Cancer Ther* 2019; 18: 2185-2193.

42 Winkler F, Kozin SV, Tong RT, Chae SS, Booth MF, Garkavtsev I *et al*. Kinetics of vascular normalization by VEGFR2 blockade governs brain tumor response to radiation: role of oxygenation, angiopoietin-1, and matrix metalloproteinases. *Cancer Cell* 2004; 6: 553-563.

43 Matsumoto S, Batra S, Saito K, Yasui H, Choudhuri R, Gadisetti C *et al*. Antiangiogenic agent sunitinib transiently increases tumor oxygenation and suppresses cycling hypoxia. *Cancer Res* 2011; 71: 6350-6359.

44 Terry S, Faouzi Zaarour R, Hassan Venkatesh G, Francis A, El-Sayed W, Buart S *et al*. Role of hypoxic stress in regulating tumor immunogenicity, resistance and plasticity. *Int J Mol Sci* 2018; 19: 3044-3063.

45 Nieto MA. Context-specific roles of EMT programmes in cancer cell dissemination. *Nat Cell Biol* 2017; 19: 416-418.

46 Ma S, Pradeep S, Hu W, Zhang D, Coleman R, Sood A. The role of tumor microenvironment in resistance to anti-angiogenic therapy. *F1000Res* 2018; 7: 326.

47 Lyons YA, Pradeep S, Wu SY, Haemmerle M, Hansen JM, Wagner MJ *et al*. Macrophage depletion through colony stimulating factor 1 receptor pathway blockade overcomes adaptive resistance to anti-VEGF therapy. *Oncotarget* 2017; 8: 96496-96505.

48 Shojaei F, Lee JH, Simmons BH, Wong A, Esparza CO, Plumlee PA *et al*. HGF/c-Met acts as an alternative angiogenic pathway in sunitinib-resistant tumors. *Cancer Res* 2010; 70: 10090-10100.

49 Jahangiri A, De Lay M, Miller LM, Carbonell WS, Hu YL, Lu K *et al*. Gene expression profile identifies tyrosine kinase c-Met as a targetable mediator of antiangiogenic therapy resistance. *Clin Cancer Res* 2013; 19: 1773-1783.

50 Huang D, Ding Y, Zhou M, Rini BI, Petillo D, Qian CN *et al*. Interleukin-8 mediates resistance to antiangiogenic agent sunitinib in renal cell carcinoma. *Cancer Res* 2010; 70: 1063-1071.

51 Kryczek I, Lange A, Mottram P, Alvarez X, Cheng P, Hogan M *et al*. CXCL12 and vascular endothelial growth factor synergistically induce neoangiogenesis in human ovarian cancers. *Cancer Res* 2005; 65: 465-472.

52 Charo DN, Ho M, Fajardo G, Kawana M, Kundu RK, Sheikh AY *et al*. Endogenous regulation of cardiovascular function by apelin-APJ. *Am J Physiol Heart Circ Physiol* 2009; 297: H1904-1913.

53 Mastrella G, Hou M, Li M, Stoecklein VM, Zdouc N, Volmar MNM *et al*. Targeting APLN/APLNR Improves Antiangiogenic Efficiency and Blunts Proinvasive Side Effects of VEGFA/VEGFR2 Blockade in Glioblastoma. *Cancer Res* 2019; 79: 2298-2313.

54 Hanahan D, Weinberg RA. Hallmarks of cancer: the next generation. . *Cell* 2011; 144: 646-674.

55 Paez-Ribes M, Allen E, Hudock J, Takeda T, Okuyama H, Vinals F *et al*. Antiangiogenic therapy elicits malignant progression of tumors to increased local invasion and distant metastasis. *Cancer Cell* 2009; 15: 220-231.

56 Soler A, Serra H, Pearce W, Angulo A, Guillermet-Guibert J, Friedman LS *et al*. Inhibition of the p110alpha isoform of PI 3-kinase stimulates nonfunctional tumor angiogenesis. *J Exp Med* 2013; 210: 1937-1945.

57 Mateo J, Ganji G, Lemech C, Burris HA, Han SW, Swales K *et al*. A first-time-in-human study of GSK2636771, a phosphoinositide 3 kinase beta-selective inhibitor, in patients with advanced solid tumors. *Clin Cancer Res* 2017; 23: 5981-5992.

Figure Legends

Figure 1. Inhibition of PI3Kβ decreases sprouting angiogenesis in HUVECs co-cultured with patient-derived renal cancer (PD-RCC) samples. **A,** Freshly-harvested PD-RCC samples were minced, then co-cultured with HUVEC spheroids with vehicle or 100 nM TGX-221 as described in Methods. Mock-treated EC cultures were used as the control (Ctrl). Scale bars 95 μm. **B,** Quantification of the number and length of angiogenic sprouts (mean ± SEM; n = 8 independent PD-RCC samples; $^{**}P < 0.01$; two-way ANOVA). **C,** Endothelial tip cell marker gene expression in PD-RCC/ EC spheroid 3D co-culture (mean ± SEM; n = 8 independent samples; $^{*}P < 0.05$; two-way ANOVA). Mock-stimulated EC spheroids were used as the reference. **D,** Quantification of pro-angiogenic growth factor expression by PD-RCC. PD-RCC samples that didn't stimulate angiogenesis were used as the reference (mean ± SEM; n = 8 independent samples; $^{*}P < 0.05$, $^{**}P<0.01$; Mann-Whitney *U* - test). **E,** Expression of VEGF and CXCL12 in PD-RCC samples by western blot.

Figure 2. Inactivation of endothelial PI3Kβ potentiates sunitinib treatment to delay tumor growth and reduce tumor vessel density. **A,** 1 X 10^6 mouse Lewis lung carcinoma (LLC1) cells were implanted subcutaneously into wild-type (Ctrl) or EC-βKO mice (n = 4 - 8 mice / group). When the tumor volume reached 200 mm^3, mice were treated with sunitinib (40mg / kg / day) or vehicle. Tumor volume was measured every 3 days using slide calipers as described in Methods. Results are presented as the mean ± SEM; $^{*}P <$

0.05, $**P < 0.01$ by two-way ANOVA, repeated measure. **B,** Representative immunohistochemical (IHC) images of $CD31^+$ vessels. Scale bar, 50 μm. **C,** Quantification of $CD31^+$ vessels per high power field (HPF) from (B) (mean ± SEM; n = 4 - 8 mice / group; $**P < 0.005$; Mann-Whitney *U* - test). **D,** Representative images of pimonidazole$^+$ hypoxic areas (scale bar, 1 mm) and **E,** quantification of tumor pimonidazole$^+$ area (mean ± SEM; n = 4 - 8 mice / group; $*P < 0.05$, $**P < 0.01$; Mann-Whitney *U* - test). **F,** hypoxia responsive marker gene expression in vehicle or sunitinib-treated control *vs* EC-βKO mice (mean ± SEM; mice n = 4 - 8 mice / group; $*P < 0.05$, $**P < 0.01$; Mann-Whitney *U* - test). **G,** NDRG1 protein level was probed by western blot in early-stage tumors collected from sunitinib-treated wild-type *vs* EC-βKO mice. **H,** Quantification of western blot images among the groups (mean ± SEM; n = 5 mice/ group; $*P < 0.05$; Mann-Whitney *U* - test).

Figure 3. Inactivation of endothelial PI3Kβ promotes tumor vessel normalization in sunitinib-treated mice. Vessel maturity was evaluated by using NG2$^+$ pericyte and Collagen IV$^+$ (Col IV) basement membrane staining. **A,** Representative images of NG2 (red) coverage of $CD31^+$ (green) tumor vessels in vehicle or sunitinib-treated wild-type (Ctrl) *vs* EC-βKO mice. Scale bar, 50 μm. **B,** Quantification of the fraction of NG2-associated $CD31^+$ vessels (mean ± SEM; n = 4-8 mice/ group; $*P < 0.05$, $**P < 0.01$; Mann-Whitney *U* - test). **C,** Representative images of $CD31^+$ (green) vessels and Col IV$^+$ (red) capillary basement membranes. Scale bar, 50 μm. **D,** Quantification of Col IV$^+$ coverage of $CD31^+$ vessel profiles (left panel), and Col IV$^+$ empty sleeves (right) in vehicle or sunitinib-treated wild-type *vs* EC-βKO mice (mean ± SEM; n = 4 - 8 mice/

group; **P < 0.01; Mann-Whitney U - test). **E,** Representative images of lectin$^+$ (red) perfused tumor vessels in sunitinib-treated wild-type *vs* EC-βKO mice. Scale bar, 20 μm. **F,** Quantification of the fraction of lectin-positive CD31$^+$ vessels (mean ± SEM; n = 5 mice/ group; **P < 0.005; Mann-Whitney U - test).

Figure 4. Inactivation of endothelial PI3Kβ reduces tumor angiogenesis. **A,** Representative images of sprouting from large vessels in sunitinib-treated wild-type (Ctrl) *vs* EC-βKO mice. The inset shows a sprout with tip cell filopodia. Scale bars, 50 μm. **B,** Quantification of angiogenic sprouts in LLC1 tumors from sunitinib-treated wild-type *vs* EC-βKO mice (mean ± SEM; n = 5 mice/ group; *P < 0.05, **P < 0.01; Mann-Whitney U - test). **C,** Quantification of endothelial tip cell marker gene expression in vehicle or sunitinib-treated wild-type *vs* EC-βKO mice (mean ± SEM; n = 4 - 8 mice/ group; *P < 0.05, **P < 0.01; Mann-Whitney U - test). **D-E,** western blot analysis of angiopoietin-2 (Ang2) protein level in early-stage tumor collected from sunitinib-treated wild-type *vs* EC-βKO mice (mean ± SEM; n = 5 mice / group; **P < 0.01; Mann-Whitney U - test).

Figure 5. Cancer cell epithelial to mesenchymal transition (EMT) is reduced in EC-βKO mice **A**, EMT marker gene expression in vehicle or sunitinib-treated wild-type (Ctrl) *vs* (mean ± SEM; mice n = 4 - 8 mice/ group; *P < 0.05, **P < 0.01; Mann-Whitney U - test). **B,** The expression of Zeb1 and Slug proteins were probed by western blot in early-stage tumors collected from sunitinib-treated wild-type *vs* EC-βKO mice. **C,**

Quantification of western blot images among the groups (mean ± SEM; n = 5 mice/ group; *$P < 0.05$; Mann-Whitney *U* - test).

Figure 6. Inactivation of endothelial PI3Kβ decreases lung metastases, tumor vessel density, and tumor hypoxia in sunitinib-treated mice. Mouse B16F10 melanoma cells (2 X 10^5) were injected into the tail vein of wild-type (Ctrl) or EC-βKO mice. Immediately after tumor cell inoculation, mice were treated with vehicle or sunitinib (40mg/ kg/ day) for 20 days, then were euthanized at day 21. **A,** Representative images of H&E stained sections showing tumor foci among vehicle or sunitinib-treated wild-type *vs* EC-βKO mice. Scale bars, 1 mm. **B,** Quantification of tumor area in H&E stained sections (mean ± SEM; n = 5 - 8 mice / group; *$P < 0.05$; Mann-Whitney *U* - test). **C,** Representative images of $CD31^+$ tumor vessels and **D,** quantification (mean ± SEM; n = 5 - 8 mice/ group; *$P < 0.05$, **$P < 0.005$; Mann-Whitney *U* - test). **E,** Representative images and **F,** quantification of $pimonidazole^+$ tumor hypoxic area among vehicle or sunitinib-treated wild-type *vs* EC-βKO mice (mean ± SEM; n = 5 - 8 mice/ group; *$P < 0.05$; Mann-Whitney *U* - test). Scale bars, 1 mm. **G,** Representative images of $PDGFRB^+$ pericyte (red) coverage of $CD31^+$ (green) tumor vessels among vehicle or sunitinib-treated wild-type *vs* EC-βKO mice. Scale bars, μm. **H,** Quantification of the fraction of $CD31^+$ vessels covered by $PDGFR\beta^+$ pericytes (mean ± SEM; n = 5 - 8 mice/ group; *$P < 0.05$; Mann-Whitney *U* - test).

1

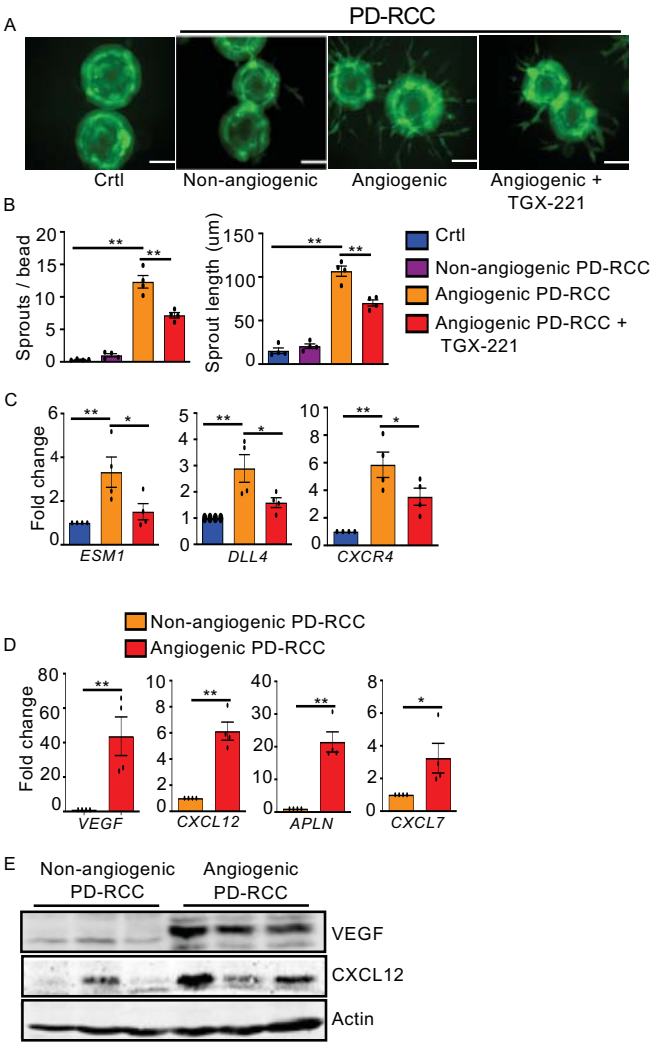
A
PD-RCC
Crtl
Non-angiogenic
Angiogenic
Angiogenic +
TGX-221
B
Sprouts / bead
Sprout length (um)
Crtl
Non-angiogenic PD-RCC
Angiogenic PD-RCC
Angiogenic PD-RCC +
TGX-221
C
Fold change
ESM1
DLL4
CXCR4
D
Non-angiogenic PD-RCC
Angiogenic PD-RCC
Fold change
VEGF
CXCL12
APLN
CXCL7
E
Non-angiogenic
PD-RCC
Angiogenic
PD-RCC
VEGF
CXCL12
Actin

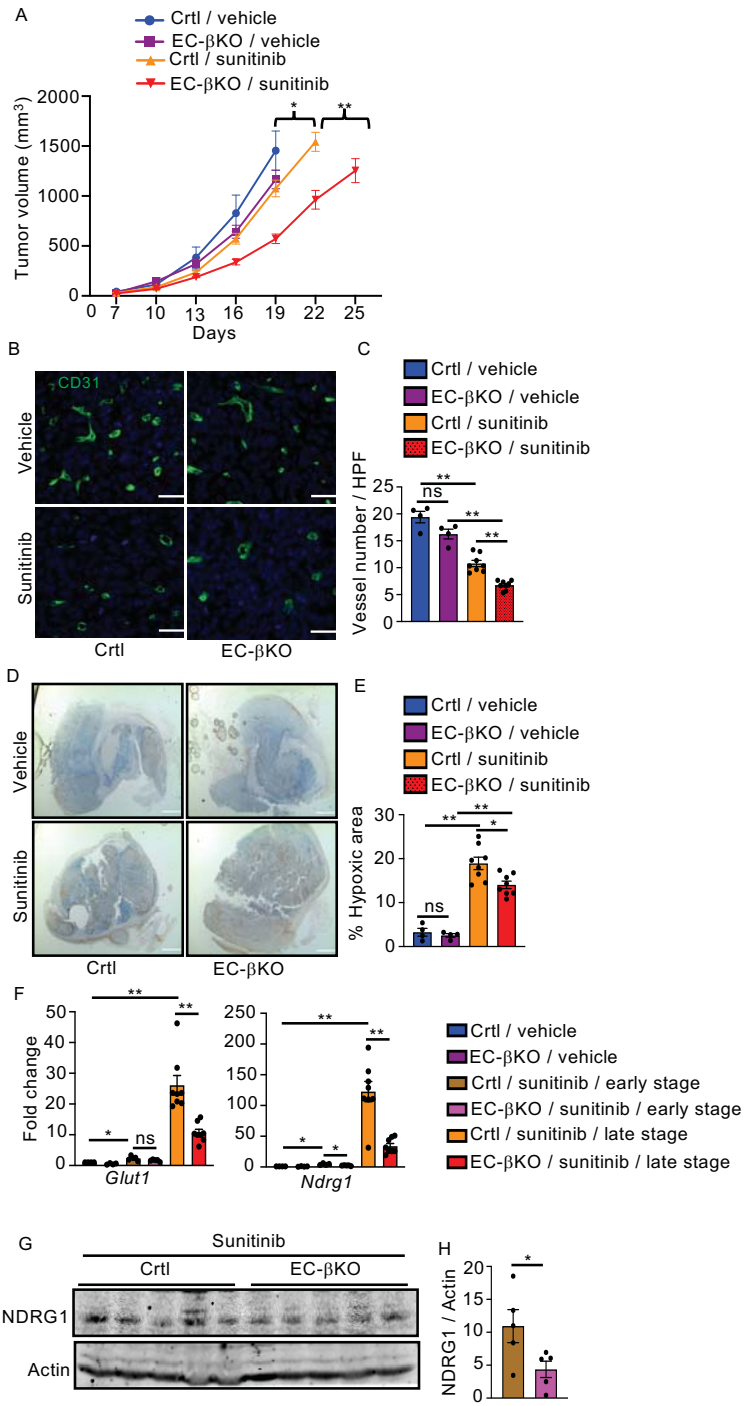
A
Crtl / vehicle
EC-βKO / vehicle
Crtl / sunitinib
EC-βKO / sunitinib
Tumor volume (mm3)
2000
1500
1000
500
0
0 7 10 13 16 19 22 25
Days
*
**
B
CD31
Vehicle
Sunitinib
Crtl
EC-βKO
C
Crtl / vehicle
EC-βKO / vehicle
Crtl / sunitinib
EC-βKO / sunitinib
Vessel number / HPF
25
20
15
10
5
0
ns
**
**
**
D
Vehicle
Sunitinib
Crtl
EC-βKO
E
Crtl / vehicle
EC-βKO / vehicle
Crtl / sunitinib
EC-βKO / sunitinib
% Hypoxic area
30
20
10
0
ns
**
**
*
F
Fold change
50
40
30
20
10
0
*
ns
**
**
Glut1
250
200
150
100
50
0
*
*
**
**
Ndrg1
Crtl / vehicle
EC-βKO / vehicle
Crtl / sunitinib / early stage
EC-βKO / sunitinib / early stage
Crtl / sunitinib / late stage
EC-βKO / sunitinib / late stage
G
Sunitinib
Crtl
EC-βKO
NDRG1
Actin
H
NDRG1 / Actin
20
15
10
5
0
*

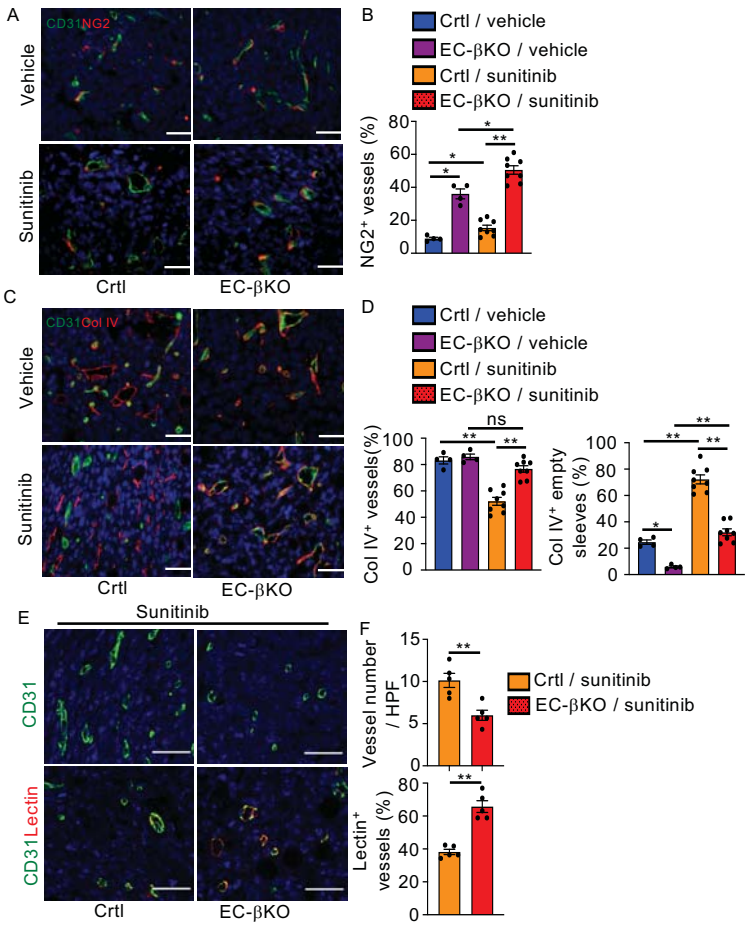
A
CD31 NG2
Vehicle
Sunitinib
Crtl
EC-βKO
B
Crtl / vehicle
EC-βKO / vehicle
Crtl / sunitinib
EC-βKO / sunitinib
NG2+ vessels (%)
C
CD31 Col IV
Vehicle
Sunitinib
Crtl
EC-βKO
D
Crtl / vehicle
EC-βKO / vehicle
Crtl / sunitinib
EC-βKO / sunitinib
Col IV+ vessels(%)
ns
Col IV+ empty sleeves (%)
E
Sunitinib
CD31
CD31 Lectin
Crtl
EC-βKO
F
Vessel number / HPF
Crtl / sunitinib
EC-βKO / sunitinib
Lectin+ vessels (%)

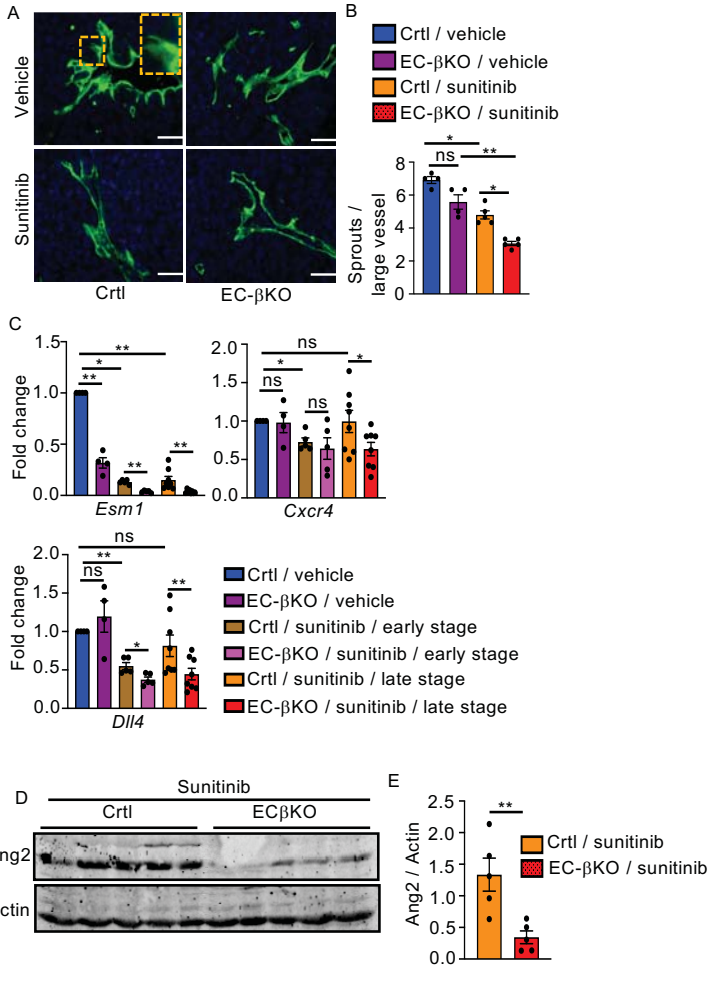
A
Vehicle
Sunitinib
Crtl
EC-βKO
B
Crtl / vehicle
EC-βKO / vehicle
Crtl / sunitinib
EC-βKO / sunitinib
Sprouts / large vessel
ns
C
Fold change
Esm1
Cxcr4
Dll4
Crtl / vehicle
EC-βKO / vehicle
Crtl / sunitinib / early stage
EC-βKO / sunitinib / early stage
Crtl / sunitinib / late stage
EC-βKO / sunitinib / late stage
D
Sunitinib
Crtl
ECβKO
Ang2
Actin
E
Ang2 / Actin
Crtl / sunitinib
EC-βKO / sunitinib

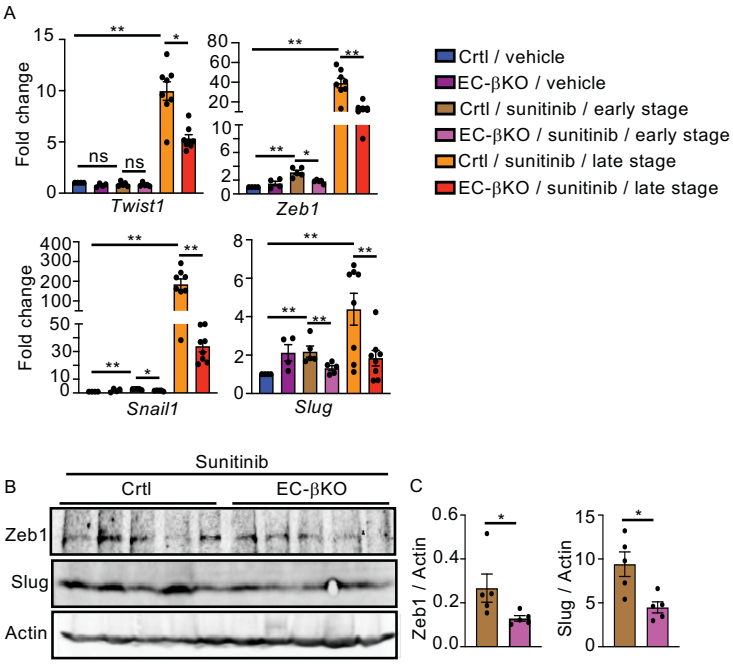
A
Fold change
Twist1
Zeb1
Snail1
Slug
ns
Crtl / vehicle
EC-βKO / vehicle
Crtl / sunitinib / early stage
EC-βKO / sunitinib / early stage
Crtl / sunitinib / late stage
EC-βKO / sunitinib / late stage

B
Sunitinib
Crtl
EC-βKO
Zeb1
Slug
Actin
C
Zeb1 / Actin
Slug / Actin

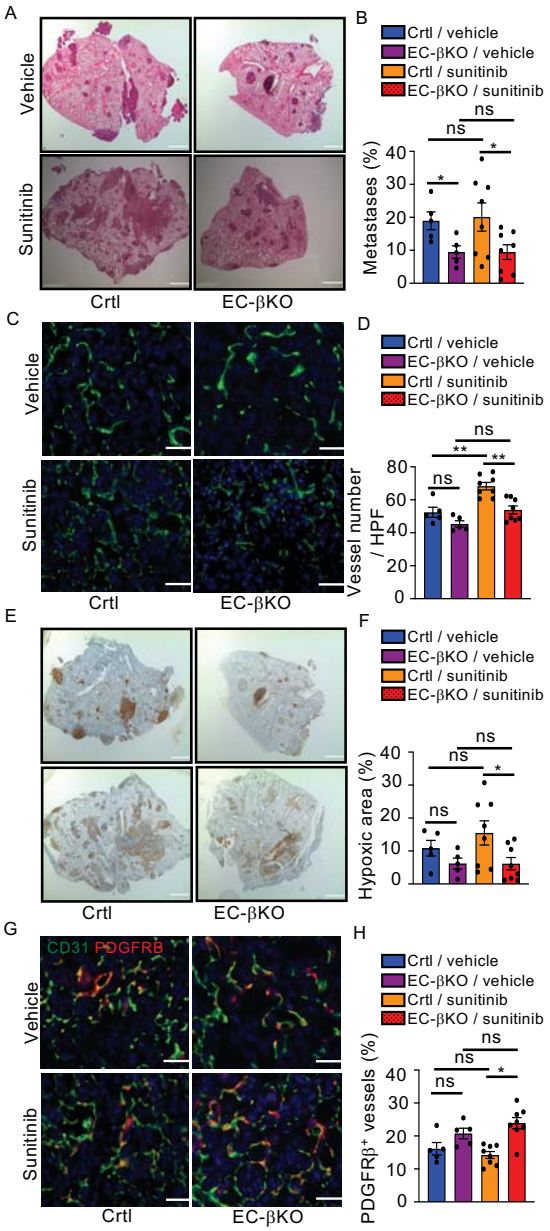
A
Vehicle
Sunitinib
Crtl
EC-βKO
B
Crtl / vehicle
EC-βKO / vehicle
Crtl / sunitinib
EC-βKO / sunitinib
Metastases (%)
ns
*
C
D
Vessel number / HPF
**
E
F
Hypoxic area (%)
G
CD31 PDGFRB
H
PDGFRβ+ vessels (%)